Sixth International Symposium on Turbulence and Shear Flow Phenomena
Seoul, Korea, 22-24 June 2009

HOMOGENEOUS TURBULENCE WITH BAROCLINIC INSTABILITY: LINEAR THEORY AND SIMULATIONS

Guillaume Simon, Fabien S. Godeferd, Claude Cambon
Université de Lyon
Laboratoire de Mécanique des Fluides et d'Acoustique
École Centrale de Lyon
F-69134 Ecully cedex, France
fabien.godeferd@ec-lyon.fr

Abdelaziz Salhi
Faculté des Sciences de Tunis
Département de Physique
1060 Tunis
Tunisia
lazizsalhi@yahoo.fr

ABSTRACT

The coupled effects of mean shear, density-stratification and system rotation are investigated in the context of strong turbulence, *i.e.* accounting for the baroclinic instability. Although there exists a large literature in the rotating shear case (e.g. [6]) and the stratified shear case, with linear approaches, Direct or Large Eddy Simulations, very few studies consider the combined three distortions.

First, one has to define an admissible flow condition for including all three effects, in order to be able to treat properly the homogeneity condition in the numerical simulations. Then, we solve numerically the complete nonlinear equations for the rotating stratified shear homogeneous turbulent flow, using a pseudo-spectral method. The most relevant parameters for these Direct Numerical Simulations (DNS) are chosen from a preliminary comprehensive parametric study that includes two simplified approaches: (a) *Rapid Distortion Theory* (RDT) with the related stability analysis technique; (b) a simplified "pressureless" stability analysis.

BASE EQUATIONS

The base conservation equations are written for a heat-conducting viscous fluid in the rotating frame of reference, under the action of gravity. It is important to make two remarks.

First, as in many geophysical applications, the centrifugal force is incorporated in an extended gravitational field $\boldsymbol{g}$, in such a way that

$$\boldsymbol{g} = -\boldsymbol{\nabla}\Phi_g - \boldsymbol{\Omega}\times(\boldsymbol{\Omega}\times\boldsymbol{x}) = -\boldsymbol{\nabla}(\Phi_g - \frac{1}{2}|\boldsymbol{\Omega}\times\boldsymbol{x}|^2)$$

where Φ_g is the natural gravitation field potential.

Second, the Boussinesq approximation yields the variation of fluid density due to a small variation of fluid temperature as

$$\rho = \rho_0(1-\beta(T-T_0))$$

where ρ_0 is the density of the fluid at the reference temperature T_0, and β is the expansion coefficient, under the condition that

$$\left|\frac{\rho-\rho_0}{\rho_0}\right| = -\beta(T-T_0) \ll 1.$$

The Boussinesq approximation provides the following equations for the fluid velocity $\boldsymbol{u}$ and the buoyancy $b\boldsymbol{e}_3 = -g(\rho-\rho_0)/\rho_0 = g\beta(T-T_0)\boldsymbol{e}_3$:

$$\boldsymbol{\nabla}\cdot\boldsymbol{u} = 0$$

$$(\partial_t + \boldsymbol{u}\cdot\boldsymbol{\nabla})\boldsymbol{u} + 2\Omega\boldsymbol{e}_3\times\boldsymbol{u} = -\boldsymbol{\nabla}\left(\frac{P}{\rho_0} + gx_3\right) + b\boldsymbol{e}_3 + \nu\nabla^2\boldsymbol{u}$$

$$(\partial_t + \boldsymbol{u}\cdot\boldsymbol{\nabla})b = \chi\nabla^2 b$$

in the frame rotating vertically about $\boldsymbol{e}_3$ and for vertical gravity g. Thermal diffusivity is χ and molecular viscosity ν.

The baroclinic torque appears upon writing the vorticity equation by taking the curl of the previous velocity equation:

$$(\partial_t + \boldsymbol{u}\cdot\boldsymbol{\nabla})\boldsymbol{\omega} = \boldsymbol{\omega}\cdot\boldsymbol{\nabla}\boldsymbol{u} + \frac{1}{\rho^2}\boldsymbol{\nabla}\rho\times\boldsymbol{\nabla}p + \nu\nabla^2\boldsymbol{\omega}$$

which, using the Boussinesq approximation, allows to write the torque as:

$$\frac{1}{\rho^2}\boldsymbol{\nabla}\rho\times\boldsymbol{\nabla}p \simeq \frac{1}{\rho^2}\boldsymbol{\nabla}(\rho-\rho_0)\times(-\rho_0 g\boldsymbol{e}_3) = \boldsymbol{\nabla}\times(-\frac{g}{\rho_0}(\rho-\rho_0)$$

$$= \boldsymbol{\nabla}\times(b\boldsymbol{e}_3).$$

In barotropic flows, both pressure and density gradients are aligned, resulting in zero additional torque. In the baroclinic case, the misalignment of $\boldsymbol{\nabla}\rho$ and $\boldsymbol{\nabla}p$ produces the baroclinic torque which is responsible for baroclinic instabilities.

THE ADMISSIBLE PROBLEM

As a first point, we emphasize the necessity to define a self-consistent, physically relevant, mathematical system to represent homogeneous turbulence subjected to space-uniform mean gradients. This leads to using *admissibility conditions*—as coined by A. C. C. Craik in the context of stability analysis):

> The mean (or base) flow must be a solution of the Euler (or Helmholtz) equations, in connection with a fluctuating (or disturbance) flow expressed in terms of Fourier modes advected by the mean flow.

Both in RDT- and DNS-related studies, the problem of admissibility is often ignored, because the numerical technique can be used regardless of the validity of the mean flow, thereby not detecting the appearance of a spurious gyroscopic torque—when not artificially balanced by an additional term. Based on this, existing studies include turbulence with a mean shear flow, rotating about the cross-gradient direction (*e.g.* [5]), with RDT applications proposed in astrophysics for protoplanetary disks or stellar convection. In the oscillating shear flow considered by Yu & Girimaji, 2005, the spurious vorticity term induced by the periodic oscillation of the shear is balanced by an artificial body force. Even if these studies include potentially interesting elements, it is better to address mean flows that are consistent with the homogeneity property of turbulence, which are exact solutions thanks to *physical* effects rather than numerical add-ons.

We consider the mean flow sketched in figure 1, consisting of mean shear with rate S, vertical vorticity with rotation rate $f = 2\Omega$, and vertical stabilizing density stratification characterized by the Brunt-Väisälä frequency N (proportional to the square root of the mean vertical density gradient). Admissibility conditions are satisfied if the Helmholtz equation for the streamwise component of absolute vorticity W_1 is

$$\frac{dW_1}{dt} - Sf = -\frac{\partial \bar{b}}{\partial x_2}. \tag{1}$$

where $\bar{b}$ is the buoyancy, *i.e.* the density flux. In the absence of an additional spanwise component of mean density—or buoyancy—gradient, mean vorticity is therefore created in the streamwise direction. Conversely, W_1 production can be balanced by the addition of the following density gradient:

$$\frac{\partial \bar{b}}{\partial x_2} = Sf = -\underbrace{\frac{Sf}{N^2}}_{\epsilon}\frac{\partial \bar{b}}{\partial x_3} \tag{2}$$

In other words, the tendency for the horizontal density gradient $\partial\bar{b}/\partial x_2$ to generate streamwise vorticity (eq. (1)) is exactly balanced by twisting the background vorticity through a gyroscopic torque (cross product of vertical vorticity and shear-related spanwise vorticity, Sf term here.) This is often called the *geostrophic adjustment* in the geophysical community (e.g. Drazin & Reid 1981.)

In the presence of the admissible mean flow, parameterized by S, f and N, the fluctuating velocity u_i' and buoyancy b' are governed by

$$\dot{u}_i' + \underbrace{Sx_3\frac{\partial u_i'}{\partial x_1} + S\delta_{i1}u_3}_{\text{Shear}} + f\epsilon_{i3j}u_j' + \frac{1}{\rho_0}\frac{\partial p'}{\partial x_i} = b'\delta_{i3} \quad ; \quad \frac{\partial u_i'}{\partial x_i} = 0 \tag{3}$$

$$\dot{b}' + \overbrace{Sx_3\frac{\partial b'}{\partial x_1}}^{\text{Shear}} = -N^2\left(u_3' - \overbrace{\epsilon u_2'}^{\text{HDG}}\right). \tag{4}$$

using a classical Boussinesq approximation that permits the coexistence of a fluctuating density field (proportional to b' here) and non-divergent velocity. The overdot holds for a substantial derivative with nonlinear advection. (Viscous/diffusive terms are omitted here for the sake of brevity.) The new terms induced by shear are underlined: two direct distortion terms (label shear) and horizontal density gradient (HDG) effects.

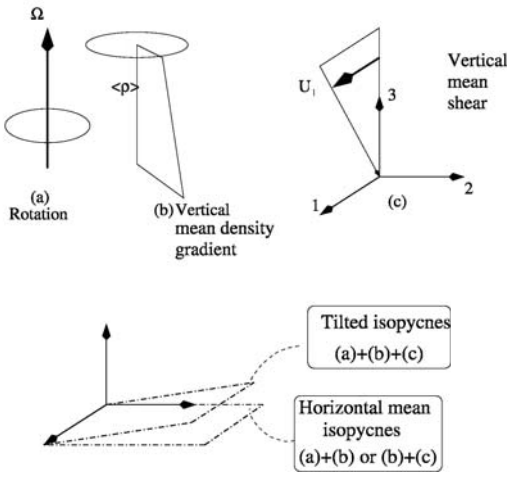

Figure 1: Sketch of the mean flow, including: (a) system vorticity; (b) vertical stable stratification; (c) mean shear. Tilting isopycnal surfaces can trigger the baroclinic instability, if (a)-(b)-(c) are simultaneously present.

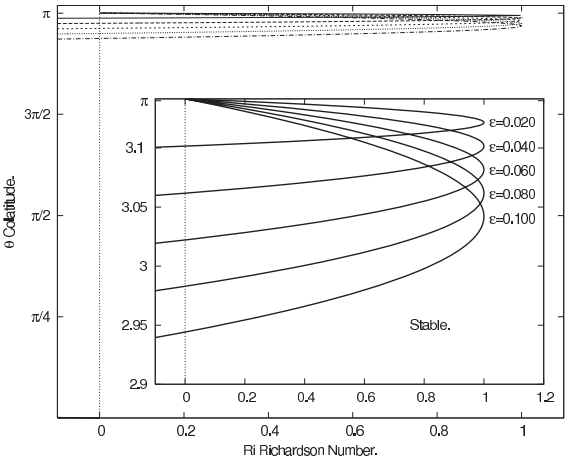

Figure 2: Neutral curves (growth rate $\omega_0 = 0$) for $k_1 = 0$: the exponentially unstable regions are delineated by the concave side of the curves. Different values of the non dimensional parameter ϵ are used.

The equation (1) is a consequence of the basic flow admissibility constraint: The slope $\epsilon = \bar{b}_{,2}/\bar{b}_{,3}$ of the mean isopycnal—constant density—surfaces is due to the coupling between shear and rotation; obviously, $\epsilon = 0$ without either shear or the Coriolis force (see figure 1.) Considering non zero ϵ is important, since it corresponds to the baroclinic instability, which can be used for a major modelling issue in meteorology: the large-scale instability of the westerly winds in mid-latitudes.

MODELS AND SIMULATIONS

Equations (3) and (4) are solved with varying two independent parameters chosen among the Rossby number $Ro = \frac{S}{f}$, the Richardson number $Ri = \frac{N^2}{S^2}$ and the baroclinic coefficient $\epsilon = \frac{Sf}{N^2}$. The study is three-fold, with methods of increasing complexity: (1) a pressureless linear approach, completely analytic, with application to Reynolds Stress Models; (2) a RDT study, in which complex effects of

fluctuating pressure are accounted for. The linear equations are solved in spectral space. (3) DNS, *i.e.* including nonlinear advection terms *w.r.t.* RDT equations, treated also in spectral space (the technique first introduced by [4]).

Pressureless analysis

A preliminary but useful analysis can be obtained for the baroclinic case when taking the linear inviscid limit of equations (3) and (4), and considering the velocity/buoyancy fluctuations around the mean. The advantage of this approximation is that the pressure is discarded and does not appear any more in the problem, whence the denomination "pressureless".

This approach can also be viewed as performing the stability analysis of the system submitted to small perturbations. It is used by [9], who get a linear system of first order differential equations in $\boldsymbol{u}$ and b, with a simple matrix of coupling coefficients involving only the Richardson number Ri and the Rossby number Ro. In classical hydrodynamic stability, one computes the eigenvalues of the system, and decides on potential instabilities depending on their real part.

Here, instability is found for $Ri < 1$ since the following eigenvalues become real with a positive one that gives the growth rate:

$$\sigma = \pm \left(-(Ri + Ro^{-2}) + \sqrt{(Ri - Ro^{-2})^2 + 4Ro^{-2}} \right)^{1/2}$$

Some statistics may then be computed analytically. For instance, the anisotropy tensor components b_{ij}, *i.e.* the deviatoric part of the Reynolds stress tensor, may be obtained. The horizontal and vertical diagonal components, in the pressureless limit, and at large time, depend on the Rossby and Richardson numbers as:

$$\tilde{b}_{11}(t \to \infty) = -1/3 + \sigma^2 \left((Ro^{-2} + \sigma^)(1 + Ro^{-2} + \sigma^2) \right)^{-1} \quad (5)$$

and

$$\tilde{b}_{33}(t \to \infty) = -2/3 - \sigma^2 (1 + Ro^{-2} + \sigma^2)^{-1} \quad (6)$$

with $\tilde{b}_{22} = -(\tilde{b}_{11} + \tilde{b}_{33})$. A plot of their dependence on the Rossby number is discussed in the following (figure 6).

RDT solutions and Direct Numerical Simulations

RDT calculations are more easily performed by using mean-flow-advected spatial variables, denoted $\boldsymbol{X}$ in physical space and $\boldsymbol{K}$ in Fourier space. Expanding the fluctuating fields of equations (3) and (4) in terms of advected Fourier modes, the divergence-free constraint is replaced by a geometric one and the pressure is solved algebraically. Hence, the initial five-component $(u'_1, u'_2, u'_3, p', b')$ problem is replaced by a three-component one, in which the velocity fluctuations are represented by two independent solenoidal components: the toroidal part $u^{(1)}(\boldsymbol{k}, t)$, and the poloidal one $u^{(2)}(\boldsymbol{k}, t)$. For mathematical convenience, we note $u^{(3)}(\boldsymbol{k}, t)$ the buoyancy spectral amplitude, so that $u^{(3)*}u^{(3)}$ is the spectral density of potential energy.

The RDT solution involves the Green's function g_{ij} of the linearized equations, which is deterministic, and is eventually used to compute statistical moments of fluctuating variables (see [8] for details.)

Additionally, the Green's function is also the main ingredient for performing the stability analysis. In short, the linearized equations (3) and (4) amount to a system

$$\dot{u}^{(i)} + m_{ij}(\boldsymbol{k}(t))u^{(j)} = 0, \ i, j, = 1, 2, 3$$

with solution

$$u^{(i)}(\boldsymbol{k}(t), t) = g_{ij}(\boldsymbol{k}, t, t_0)u^{(j)}(\boldsymbol{k}(t_0), t_0)$$

and $\boldsymbol{k}(t_0) = \boldsymbol{K}$.

For $k_1 = 0$, which corresponds to infinitely elongated physical structures in the streamwise direction, the inviscid RDT solution is obtained analytically in terms of a $\boldsymbol{k}$-dependent frequency ω_0. These solutions exhibit an oscillating behavior (stable case) when $\omega_0^2 > 0$, an exponential growth (unstable case) whenever $\omega_0^2 < 0$, and a linear (algebraic) growth if $\omega_0 = 0$. Neutral curves drawn in the (R_i, $\theta = \widehat{(\boldsymbol{k}, \boldsymbol{n})}$) plane for $k_1 = 0$ for different values of ϵ are displayed in figure 2. The plot shows the neutral curves in the Ri,θ plane, in which θ corresponds to the orientation of the wavevector of the most unstable mode. The inset close-up shows small values of ϵ, which are more relevant for geophysical applications.

Among the attempts at modelling baroclinic flows, the analysis by Eady (1949) [10] considered only the geostrophic mode at vanishing Rossby number $Ro \to 0$. The computed RDT solution at $k_1 \neq 0$ yields amplification rates which are comparable to those found by Eady for small values of the parameter ϵ. Further RDT computations for $k_1 \neq 0$ demonstrate that the instability is concentrated near $k_1 = 0$.

The model by Stone [12] included the non geostrophic part of the fluid motion, and a more complete model was proposed by Molemaker et al. [11], to include both the geostrophic and the ageostrophic modes at Burger number $B = Ro^2 Ri = 1$. They show that at $Ri < 1$, the centrifugal instability occurs both for symmetric and for non symmetric perturbations.

Direct numerical simulations (DNS) of the system of equations (3) and (4) are performed with a classical pseudo-spectral method (see *e.g.* [1] for details). The fluctuating fields are developed on a basis of Fourier modes in the three spatial directions, and the equations for the spectral coefficients, derived from the equations in physical space, are written in a Lagrangian framework attached to the deformable k-space, due to shear. Periodic remeshing is required to restore the skewed computational box to a cube, an operation that does not seem to induce significant energy loss. Full de-aliasing is performed when treating the nonlinear terms by direct and inverse Fourier-transforms. Finally, a second-order accurate time-stepping is applied. The resulting velocity and temperature fields are then either plotted in three-dimensional space to observe the structure of turbulence, or used to compute a series of statistical quantities: energies, Reynolds stress tensor components, anisotropy tensor, integral length scales, *etc.*

RESULTS

The complete study allows us to compare the evolutions of the energies obtained from the pressureless analysis, full RDT, and from DNS. We show that the threefold coupling between shear, rotation and stratification stretches the instability region up to $Ri = 1$. Without system rotation, the instability essentially concerns negative values of the Richardson number, and is limited by rather small positive values of Ri: $R_i \sim 0.1$ is observed in results coming from RDT, DNS, and LES. DNS simulations are carried out to complete and confirm the RDT results.

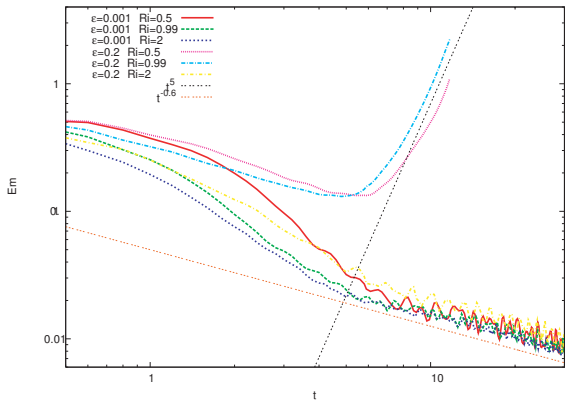

Figure 3: Evolution of the kinetic energy in the 128^3 DNS for several parametric cases, combining the values of $\epsilon = 0.001$ and $\epsilon = 0.2$ to Richardson numbers $Ri = 0.5, 0.99, 2$. The two unstable cases correspond to $\epsilon = 0.2$ and $Ri = 0.99$ and $Ri = 0.5$.

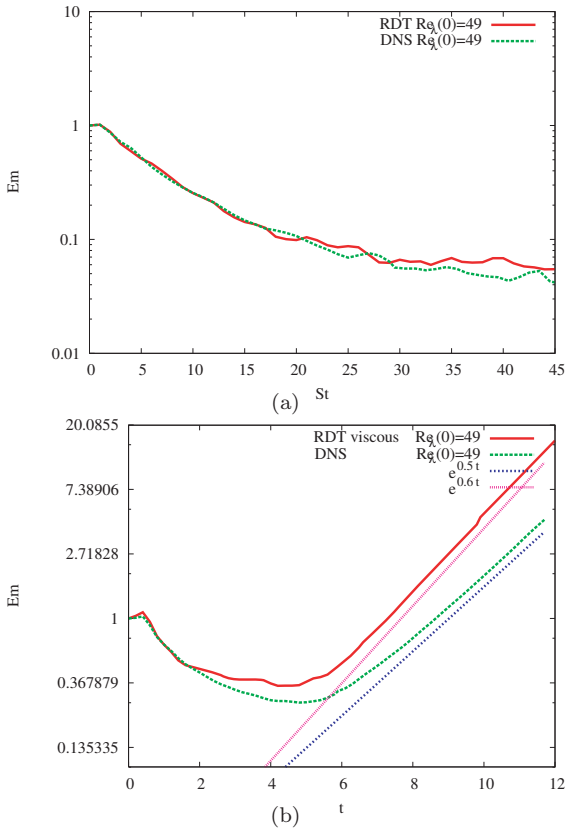

Figure 4: Time evolution of the kinetic energy computed by RDT computations with viscosity and 128^3 DNS at $Re_\lambda = 49$: (a) $\epsilon = 0.2$, $Ri = 2$; (b) $\epsilon = 0.2$, $Ri = 0.99$.

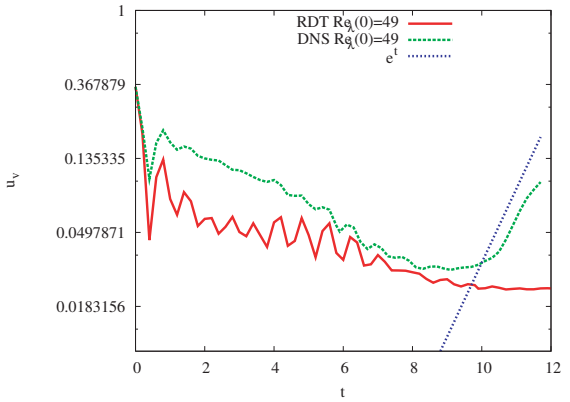

Figure 5: Compared time evolution of the vertical velocity component u_3 provided by RDT and 128^3 DNS computations for the parametric case $\epsilon = 0.2$, $Ri = 0.99$.

In figure 3, we have explored the ϵ,Ri parametric space, in order to quantify the evolution of the kinetic energy computed by DNS. The result is quite clear: while the cases at $Ri > 1$ remain stable whatever the value of ϵ, the cases at $Ri < 1$ exhibit a growth of the kinetic energy under the baroclinic instability only for significant enough $\epsilon = 0.2$. When looking at the neutral curves on figure 2, the unstable domain at small ϵ appears to be very limited, and is probably not captured in the discretized space of the simulations. For a not too small value of ϵ, the simulation reproduces correctly the exponential growth of the baroclinic instability.

The curves of figure 4 again show the evolution of the kinetic energy from the isotropic initial conditions, this time computed by both viscous RDT and DNS, for two parametric cases at $\epsilon = 0.2$: $Ri = 2$ and $Ri = 0.99$. As expected, the first case (figure 4a) exhibits a steady decay of the kinetic energy, and not much difference between the linear model and the full nonlinear simulations at this moderate $Re^\lambda = 49$ value.

In the case at $Ri = 0.99$ (figure 4b), the instability is present and captured by both RDT and DNS, although the growth rate is larger in the former model. This may be explained by the presence of the nonlinear energy transfer terms that start cascading a part of the energy produced by the instability at different scales than the primary instability mode, and therefore drain part of the energy out of this mode.

In this last case, it is interesting to note that, although the energy growth seems similar in both the linear model and the DNS, the structuration of the field differs completely. Obviously, the lack of nonlinear terms automatically prevents the creation of skewness in the velocity field computed by RDT. This is shown on the plot of figure 5 that shows the time evolution of the vertical velocity component u_3, from the initial isotropic conditions at $t = 0$. The RDT curve exhibits larger amplitudes oscillations than the DNS, in which u_3 grows strongly after a given time, corresponding to the creation by the baroclinic instability of strong three-dimensional coherent structures which do not appear in the linear model.

The anisotropy of the Reynolds stress tensor can still be partly predicted by a linear approach, either pressureless analysis (equations (5) and (6)), or the RDT model. It then reflects some structuring effects, even if it may miss the aforementioned three-dimensional coherent structures shown in DNS snapshots. The dependence of the b_{ij}s on the Rossby number can therefore be obtained, and shown

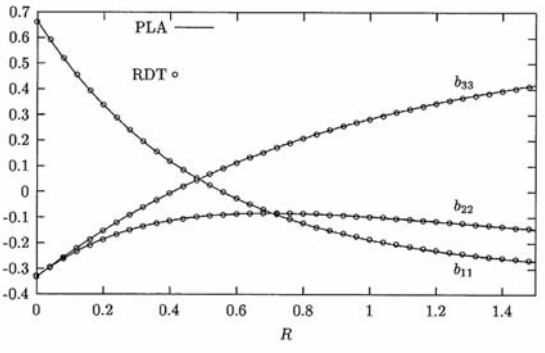

Figure 6: Deviatoric part of the Reynolds stress tensor, *i.e.* the anisotropy tensor components $b_{ij} = \overline{u_i u_j}/\overline{u_n u_n} - \delta_{ij}/3$, showing a strong growth of the vertical diagonal component b_{33}. The horizontal axis bears the inverse of the Rossby number Ro^{-1}.

on figure 6. The agreement is very good between the pressureless approximation and the RDT model, showing that pressure does not play an explicit role in the growth of the instability. The growth of b_{33} at increasing Ro also denotes the increasing production of kinetic energy.

A typical structuration of the buoyancy field, obtained by 256^3 DNS, is shown in figure 7a, comparing the structure of our sheared rotating stratified velocity field to that of the purely stratified case obtained by Riley and deBruynkop (figure 7b): DNS forced by baroclinic instability exhibit horizontal layering with Kelvin-Helmholtz-type structures, that resembles that in a purely vertically stratified flow at sufficiently high Reynolds number.

CONCLUSION

This study of baroclinic turbulence was performed using approaches ranging from a very simple analytical pressureless analysis to full non linear DNS, with an intermediate Rapid Distortion Model that can be assimilated to classical hydrodynamic stability analysis.

We have shown that interesting information can be obtained on the energetics of the baroclinic flow both by the pressureless approach and by RDT, and trends obtained on single point quantities such as Reynolds stress tensor anisotropy. Limits of stability in terms of the parameters—Richardson number Ri and baroclinic parameter ϵ—can be obtained with the linearized model, and pave the way to full DNS thanks to a comprehensive preliminary parametric study.

We show however that the complete structuration of baroclinic turbulence can only be observed in its three-dimensional extent by Direct Numerical Simulations, provided the right parameters are chosen. Moreover, the structuration of the layers is similar to that of stably stratified turbulence, but for the tilting of the layers, that is of course only present from the coupling of the three effects that produce the baroclinic torque: rotation, shear, density gradient.

The study will be pursued to assess the amount of intermittency of baroclinic turbulence, and therefore will need to reach higher values of the Reynolds number using parallel computations.

Acknowledgments

The simulations have been performed thanks to CPU time allocated by IDRIS, a computing center operated by the french National Center for Scientific Research (CNRS), under project number 071851.

*

References

[1] G. Simon, Ph. D. thesis, Université de Lyon (2007)

[2] G. K. Batchelor and I. Proudman, *The effect of rapid distortion in a fluid in turbulent motion,* Q. J. Mech. Appl. Math. **7**, 83–103 (1954)

[3] F. S. Godeferd, C. Cambon, S. Leblanc, *Zonal approach to centrifugal, elliptic and hyperbolic instabilities in Suart vortices with external rotation,* J. Fluid Mech. **449**, 1–37 (2001)

[4] R. Rogallo, NASA Tech. Mem. No. 81315 (1981)

[5] F. G. Jacobitz, *Effect of shear and rotation on turbulence flow in a stratified fluid,* Fourth Int. Symp. on Turb. Shear Flow Phen. , Williamburg, VA, USA (2005)

[6] A. Salhi & C. Cambon, *An analysis of rotating shear flow using using linear theory and DNS and LES results* J. Fluid. Mech. **347**, 171–195 (1997)

[7] A. Salhi & C. Cambon, *Advances in rapid distortion theory: From rotating shear flows to the baroclinic instability.* J. App. Mech. **73**, 449 (2006)

[8] P. Sagaut & C. Cambon, *Homogeneous Turbulence Dynamics*, CUP (2008)

[9] M. Timoumi & A. Salhi, *Equilibrium states in homogeneous turbulence with baroclinic instability.*, Theor. and Comp. Fluid Dyn., submitted, 2009.

[10] E.T. Eady, *Long waves and cyclone waves.* Tellus **1**, 3352, (1949)

[11] M.J. Molemaker, J.C. McWilliams & I. Yavneh, *Baroclinic instability and loss of balance.* J. Phys. Ocean., **35**, 1505, (2005)

[12] P.H. Stone, *on non-geostrophic baroclinic instability: Part II.* J. Atmos. Sc. **27**, 721 (1970)

[13] J.J. Riley & S. M. deBruynKops. *Dynamics of turbulence strongly influenced by buoyancy.* Phys. Fluids, **15**, 2047, (2003)

Sixth International Symposium on Turbulence and Shear Flow Phenomena
Seoul, Korea, 22-24 June 2009

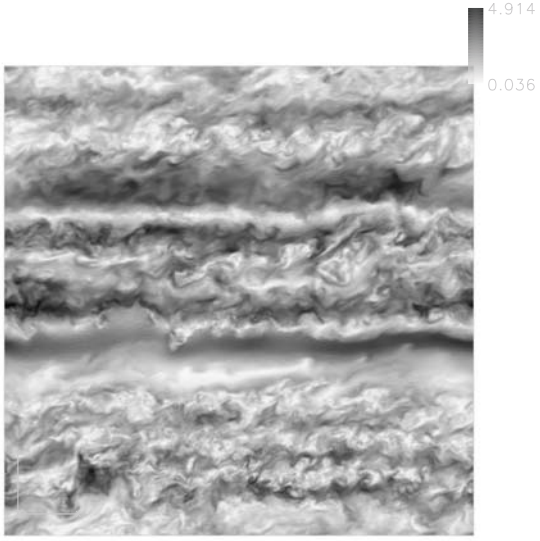

(a)

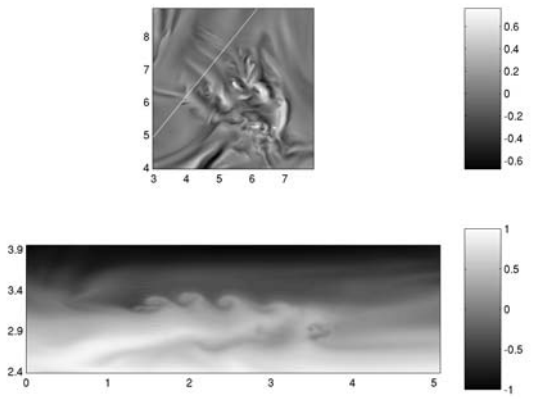

(b)

Figure 7: (a) isosurfaces of the buoyancy fluctuation in the zonal spanwise-vertical plane, from DNS at $\epsilon = 0.2$, $Ri = 0.99$, $Re_\lambda(t = 0) = 66$. (b) High Reynolds number DNS results of Riley & de Bryunkops, 2003, for stably stratified turbulence without mean shear or mean horizontal density gradient. The top panel shows part of a horizontal slice through the vertical velocity; the bottom panel shows the density on a vertical slice along the white dashed line.